Thermoacoustic mixture separation with an axial temperature gradient

D. A. Geller[a] and G. W. Swift
Condensed Matter and Thermal Physics Group, Los Alamos National Laboratory, MS K764, Los Alamos, New Mexico 87545

(Received 2 October 2008; revised 17 February 2009; accepted 19 February 2009)

The theory of thermoacoustic mixture separation is extended to include the effect of a nonzero axial temperature gradient. The analysis yields a new term in the second-order mole flux that is proportional to the temperature gradient and to the square of the volumetric velocity and is independent of the phasing of the wave. Because of this new term, thermoacoustic separation stops at a critical temperature gradient and changes direction above that gradient. For a traveling wave, this gradient is somewhat higher than that predicted by a simple four-step model. An experiment tests the theory for temperature gradients from 0 to 416 K/m in 50–50 He–Ar mixtures.
 [DOI: 10.1121/1.3097767]

PACS number(s): 43.35.Ud, 43.20.Mv, 43.35.Ty [RR] Pages: 2937–2945

I. INTRODUCTION

When sound propagates through a gas mixture confined within a duct, the mixture partially separates, creating gradients in the concentrations of its components along the length of the duct.[1–4] This thermoacoustic separation is due to the oscillating, combined effects of viscosity and thermal diffusion, with appropriate phasing, in the acoustic boundary layer. The thermoacoustic separation mechanism is similar to that employed in a conventional thermal-diffusion column,[5] except for three major differences. First, the radial temperature gradient and thermal diffusion are oscillating in the case of thermoacoustic separation but are steady in the case of conventional thermal diffusion. Second, the temperature excursions δT in thermoacoustic separation, which are due to the adiabatic compressions and rarefactions in the acoustic wave, are small compared to the absolute mean temperature of the gas; in thermal-diffusion columns, though, the temperature difference δT between the walls of the column is generally comparable to the absolute mean temperature. Third, the bulk gas motion that yields large mole-fraction differences $\Delta n \gg k_T \delta T$ (where k_T is the thermal-diffusion ratio) occurs due to acoustically driven, oscillating motion of the gas in thermoacoustic separation, instead of being driven steadily by natural convection as in a thermal-diffusion column, allowing thermoacoustic separation to work with any orientation of the duct, in a coiled or folded duct, or even in the absence of gravity.

Since thermoacoustic separation depends on thermal diffusion, it is important to investigate the effect of an axial temperature gradient. For example, if a separation duct is to be operated at elevated temperatures, one would need to know whether the entire duct must be subjected to high temperatures or whether it is possible to have the feedstock inlet, product outlets, or acoustic drivers reside outside the hot region.

In Secs. II–IV, we revisit the previous derivations[1,2,4] of thermoacoustic separation including now a finite temperature gradient lengthwise along the duct. We show in Sec. II by a simple model that there is a limiting temperature gradient at which the separation process ceases. In Secs. III and IV, we derive the mathematical details of the temperature gradient's effect on the separation. Then, in Sec. V, we describe an experimental apparatus designed for testing the theory, and we conclude in Sec. VI by showing data for separation in 50–50 He–Ar mixtures compared with the theory. The effect of the nonzero axial temperature gradient is small, but not negligible, for the conditions in these experiments.

II. THE BUCKET-BRIGADE MODEL

As has been shown previously,[1–4] the time-averaged thermoacoustic mixture-separation flux occurs due to processes in the acoustic boundary layer. To gain some intuitive understanding of the process in the presence of an axially imposed temperature gradient, we present an updated caricature of the process in Fig. 1. This figure is similar to Fig. 1 of Ref. 2, except that now the boundary carries a time-averaged axial temperature gradient dT_m/dx, whereas it was spatially isothermal in Ref. 2. The duct wall still has sufficiently large specific heat and thermal conductivity with respect to the gas that its temperature is considered to be fixed in time for any location x along the duct.

When thermoacoustic separation occurs, the time-averaged separation flux is carried by the gas parcels located approximately one thermal penetration depth δ_κ from the boundary, because those parcels experience both thermal diffusion and motion, with appropriate phasing. For such a parcel, the oscillating temperature amplitude is approximately $|T_1| = |p_1|/\rho_m c_p = (\gamma - 1) T_m |p_1|/\gamma p_m$ due to the approximately adiabatic compressions and rarefactions of the gas. In this expression, $|p_1|$ is the pressure amplitude of the sound wave, ρ_m and p_m are the mean density and pressure of the gas, c_p is the isobaric specific heat, and γ is the ratio of the isobaric and isochoric specific heats. The resulting lateral thermal

[a]Author to whom correspondence should be addressed. Electronic mail: dgeller@lanl.gov

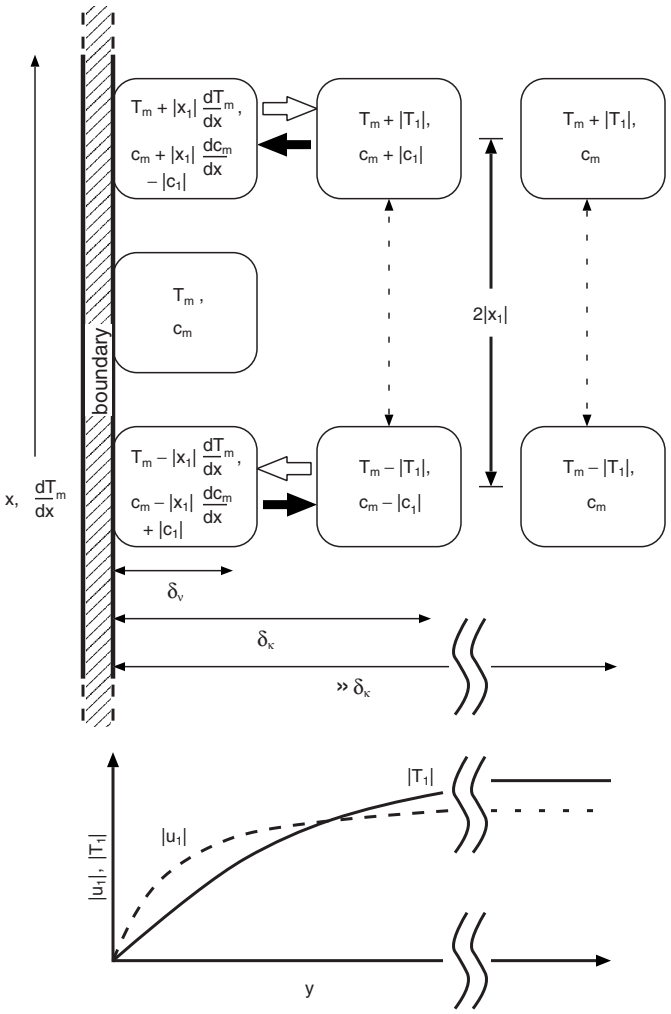

FIG. 1. Discrete time-step model of thermoacoustic separation in a binary mixture, assuming standing-wave phasing and including the effect of a temperature gradient along the duct. The three parcels of gas closest to the wall are locked in place by viscosity, but they each have different mean temperatures due to the thermal gradient along the duct. On the right-hand side of the figure, far from the wall of the duct, one parcel of gas is shown at the extrema of its motion. This parcel experiences no lateral temperature gradient during the motion, because it is outside the thermal boundary layer, as depicted in the bottom portion of the figure. In the middle of the figure, another parcel of gas is shown at the extrema of its motion near the edge of the thermoviscous boundary layer. At the extremes of its motion, there is a temperature gradient between this parcel and the parcels adjacent to the wall, driving thermal diffusion between this parcel and those at the wall. If $dT_m/dx>0$ for the phasing between motion and pressure considered here, then the lateral thermal gradient, and therefore also the thermal diffusion between the parcels, is lower than it would be for an isothermal boundary.

gradient is determined by this temperature amplitude, by the parcel's distance from the wall, and by the axial displacement amplitude $|x_1|$ of the parcel:

$$\frac{\partial T}{\partial y} \sim \frac{|T_1| - |x_1|\frac{dT_m}{dx}}{\delta_\kappa}. \tag{1}$$

Thermal diffusion will not take place between the moving parcel and a parcel at the same x-location at the boundary when there is no temperature difference between these parcels, i.e., when Eq. (1) is zero. Therefore, thermoacoustic separation ceases when the axial thermal gradient is approximately

$$\left.\frac{dT_m}{dx}\right|_{\text{crit}} = \frac{|T_1|}{|x_1|} = \frac{\gamma-1}{\gamma} T_m \frac{|p_1|}{p_m}\frac{\omega}{|\langle u_1\rangle|}, \tag{2}$$

where ω is the angular frequency and $|\langle u_1\rangle| = \omega|x_1|$ is the amplitude of the spatially averaged velocity. This is exactly the condition defining the critical temperature gradient that differentiates thermoacoustic engines and refrigerators.[6] In the simple model of Fig. 1, we are following the oscillating flow of molecules instead of heat. However, since both of these flows are driven by a lateral temperature gradient, the axial gradient dT_m/dx at which both processes stop must be the same. For higher gradients, thermoacoustic separation will work in the opposite direction, e.g., typically causing a time-averaged flux of the lighter component opposite to the direction of acoustic power flow, analogous to the change in direction of time-averaged enthalpy flow as a thermoacoustic refrigerator is taken past its critical temperature gradient to become an engine.

Similar to our previous calculation of the saturation gradient in Ref. 2, we define $(dT_m/dx)_{\text{crit}}$ exactly as in Eq. (2), and we define

$$\Gamma_T = \frac{dT_m/dx}{(dT_m/dx)_{\text{crit}}} \tag{3}$$

as a dimensionless measure of the temperature gradients in what follows. Although in general this real number could have any magnitude, in our experiments $-1<\Gamma_T<1$.

III. DEVELOPMENT OF THE FIRST-ORDER EQUATIONS

To calculate the effect of an axial temperature gradient, we follow the notation and approach of Swift and Spoor[1] by expanding the thermoacoustic variables to first order in the time dependence

$$p = p_m + \Re[p_1(x)e^{\imath\omega t}], \tag{4}$$

$$u = \Re[u_1(x,r)e^{\imath\omega t}], \tag{5}$$

$$T = T_m(x) + \Re[T_1(x,r)e^{\imath\omega t}], \tag{6}$$

$$\rho, c, s: \text{ similar to } T, \tag{7}$$

where x is the axial coordinate along the duct, s is the entropy per unit mass, c is the mass fraction of the heavier component, $\Re[]$ denotes the real part, and $\imath=\sqrt{-1}$. The mean temperature T_m was independent of x in Ref. 1.

The diffusive mass-flux density vector is given by Landau and Lifshitz[7] as

$$\mathbf{i} = -\rho D_{12}\left[\nabla c + \frac{k_T'}{T}\nabla T\right], \tag{8}$$

where D_{12} is the mutual diffusion coefficient and k_T' is the mass-scaled thermal-diffusion ratio. The convection and diffusion of the mass fraction c is then

$$\rho\left(\frac{\partial c}{\partial t}+\mathbf{u}\cdot\nabla c\right)=-\nabla\cdot\mathbf{i}=\nabla\cdot\left[\rho D_{12}\left(\nabla c+\frac{k_T'}{T}\nabla T\right)\right]. \tag{9}$$

Inserting the expansions of Eqs. (4)–(7) and keeping only the first-order oscillating quantities, one might consider new terms containing spatial derivatives of T_m or ρ_m that are nonzero due to the gradients in temperature and concentration, such as $-\rho_1 D_{12} k_T'(1/T_m\cdot dT_m/dx)^2$. Those new terms can be neglected because they are of order $(\delta_\kappa/\lambda)^2$ smaller than other terms, where λ is the wavelength, leaving

$$c_1+\frac{u_1}{\imath\omega}\frac{dc_m}{dx}=\frac{\delta_D^2}{2\imath}\left[\nabla_r^2 c_1+\frac{k_T'}{T_m}\nabla_r^2 T_1\right], \tag{10}$$

where $\delta_D=\sqrt{2D_{12}/\omega}$ is the mass diffusion length, which is unchanged from Eq. (18) of Ref. 2. Although the temperature gradient is nonzero, it does not affect the convection and diffusion in the mixture through this first-order equation. (Nevertheless, the gradient dT_m/dx does influence mass flow at *zeroth* order through the steady thermal diffusion in the x direction; this will be seen in the expression for the total separation flux in Sec. IV.)

The oscillating heat transfer in the mixture is given by Eq. (20) of Ref. 1:

$$\rho_m T_m\left(\imath\omega s_1+u_1\frac{ds_m}{dx}\right)=k\nabla_r^2 T_1-\left[k_T'\left(\frac{\partial g}{\partial c}\right)_{p,T}-T_m\left(\frac{\partial g}{\partial T}\right)_{p,c}\right]\nabla\cdot\mathbf{i}_1, \tag{11}$$

where k is the thermal conductivity and g is the Gibbs free energy per unit mass of the mixture, and the divergence of the first-order oscillating mass flux is

$$\nabla\cdot\mathbf{i}_1=-\imath\omega\rho_m c_1-\rho_m u_1\frac{dc_m}{dx} \tag{12}$$

from the left-hand side of Eq. (9). The entropy terms are replaced using the differential identity

$$ds=\frac{c_p}{T}dT-\left(\frac{\partial g}{\partial T}\right)_{p,c}dc-\frac{1}{\rho T}dp \tag{13}$$

from Eq. (22) of Ref. 1. In the case of ds_m/dx, though, we now must keep both the dT_m/dx and dc_m/dx contributions, while the dp_m/dx part remains zero since there is no mean pressure gradient along the duct. Using Eq. (13) to replace ds_m/dx and s_1 in Eq. (11), and using

$$\varepsilon\equiv\frac{(k_T')^2}{T_m c_p}\left(\frac{\partial g}{\partial c}\right)_{p,T}=\frac{\gamma-1}{\gamma}\frac{k_T^2}{n_H(1-n_H)} \tag{14}$$

as originally defined by Ref. 1 and in which n_H is the mole fraction of the heavier component and k_T is the thermal-diffusion ratio, we find

$$T_1=\frac{p_1}{\rho_m c_p}+\frac{\varepsilon T_m}{k_T'}c_1+\frac{\delta_\kappa^2}{2\imath}\nabla_r^2 T_1+\frac{\varepsilon T_m}{k_T'}\frac{dc_m}{dx}\frac{u_1}{\imath\omega}-\frac{dT_m}{dx}\frac{u_1}{\imath\omega} \tag{15}$$

after some cancellations. There is only one new term, featuring dT_m/dx, and it is in phase with the concentration-gradient term previously derived.[2]

Solving Eq. (15) for c_1, we substitute the result in Eq. (10) to find

$$T_1=\frac{p_1}{\rho_m c_p}+\frac{1}{2\imath}[\delta_\kappa^2+\delta_D^2(1+\varepsilon)]\nabla_r^2 T_1+\frac{\delta_\kappa^2\delta_D^2}{4}\nabla_r^4 T_1-\frac{dT_m}{dx}\frac{u_1}{\imath\omega}-\frac{\delta_D^2}{2\imath}\left(\frac{\varepsilon T_m}{k_T'}\frac{dc_m}{dx}-\frac{dT_m}{dx}\right)\frac{1}{\imath\omega}\nabla_r^2 u_1. \tag{16}$$

Making use of the general expression for the velocity in the duct,

$$u_1=\frac{\langle u_1\rangle}{1-f_\nu}(1-h_\nu), \tag{17}$$

where h_ν is a function describing the shape of the velocity profile across the duct and $f_\nu=\langle h_\nu\rangle$ is the average of this function over the cross section, we can rewrite Eq. (16) as

$$T_1=\frac{p_1}{\rho_m c_p}-\frac{\langle u_1\rangle}{\imath\omega}\frac{1}{1-f_\nu}\frac{dT_m}{dx}+\frac{1}{2\imath}[\delta_\kappa^2+\delta_D^2(1+\varepsilon)]\nabla_r^2 T_1+\frac{\delta_\kappa^2\delta_D^2}{4}\nabla_r^4 T_1+\frac{\langle u_1\rangle}{\imath\omega}\frac{1}{1-f_\nu}\frac{dT_m}{dx}h_\nu+\frac{\delta_D^2}{2\imath}\left(\frac{\varepsilon T_m}{k_T'}\frac{dc_m}{dx}-\frac{dT_m}{dx}\right)\frac{\langle u_1\rangle}{\imath\omega}\frac{1}{1-f_\nu}\nabla_r^2 h_\nu, \tag{18}$$

a result which is not limited to a particular duct geometry if ∇_r^2 is taken to be the two-dimensional Laplacian operator in the plane perpendicular to x. This equation is the same as that derived in Ref. 2, except that two new terms appear in the inhomogeneous part that are proportional to dT_m/dx. One of these terms is proportional to the velocity u_1, and the other is proportional to $\nabla^2 u_1$.

This fourth-order differential equation is to be solved for the same boundary conditions as in the previous work. Although the boundary is no longer spatially isothermal, we still assume that its specific heat and thermal conductivity are much larger than that of the gas, so that the boundary at any position x is temporally isothermal. In this case, the amplitude $T_1=0$ at the solid wall, just as it was in the case of the isothermal boundary. The other boundary conditions are that T_1 remains finite everywhere in the duct, and that the diffusive flux into the solid wall is zero:

$$i_r|_{\text{wall}}\propto\left[\nabla_r c_1+\frac{k_T'}{T_m}\nabla_r T_1\right]_{\text{wall}}=0. \tag{19}$$

Using Eqs. (15) and (17), this zero-flux boundary condition becomes

$$\left[(1+\varepsilon)\nabla_r T_1 - \frac{\delta_\kappa^2}{2\imath}\nabla_r^3 T_1 + \left(\frac{\varepsilon T_m}{k_T'}\frac{dc_m}{dx} - \frac{dT_m}{dx}\right)\frac{\langle u_1\rangle}{\imath\omega}\frac{1}{1-f_\nu}\nabla_r h_\nu\right]_{\text{wall}} = 0. \quad (20)$$

In order to calculate the derivatives needed for solving the differential equation, we now have to specify the geometry of the duct. For direct comparison with Ref. 2, it is useful to consider the boundary-layer limit, for which

$$h_\nu = e^{-(1+\imath)y/\delta_\nu} \quad \text{and} \quad f_\nu = \frac{(1-\imath)\delta_\nu}{2r_h}, \quad (21)$$

where r_h is the hydraulic radius,[8] $\delta_\nu = \sqrt{2\mu/\omega\rho_m}$ is the viscous penetration depth, and μ is the dynamic viscosity. Because it is of more practical interest, though, we also solve the problem for the case of a circular tube of arbitrary radius R. In that case,

$$h_\nu = \frac{J_0[(\imath-1)r/\delta_\nu]}{J_0[(\imath-1)R/\delta_\nu]} \quad \text{and}$$

$$f_\nu = \frac{2J_1[(\imath-1)R/\delta_\nu]}{J_0[(\imath-1)R/\delta_\nu](\imath-1)R/\delta_\nu}, \quad (22)$$

where the J_i are the usual cylindrical Bessel functions. Calculations based on the Bessel-function solution will be compared with experimental data in Sec. VI.

One may show by substitution that the solution of Eq. (18) is of the form

$$T_1 = \frac{p_1}{\rho_m c_p}\left[1 - \frac{\rho_m c_p}{p_1}\frac{\langle u_1\rangle}{\imath\omega}\frac{1}{1-f_\nu}\frac{dT_m}{dx} - Bh_\nu - Ch_{\kappa D} - \left(1 - \frac{\rho_m c_p}{p_1}\frac{\langle u_1\rangle}{\imath\omega}\frac{1}{1-f_\nu}\frac{dT_m}{dx} - B - C\right)h_{D\kappa}\right], \quad (23)$$

where the coefficient of the last term was determined by the boundary condition $T_1|_{\text{wall}}=0$, and the h_i are defined as in Eq. (21) or Eq. (22) but with different length scales δ_i defined below. In the previous solution[2] without a temperature gradient, the r- or y-independent part of T_1 was simply the oscillating temperature due to the adiabatic pressure oscillations of the gas in the sound wave. Here, we have an additional term due to the motion of gas along the temperature gradient. Since $\langle u_1\rangle/\imath\omega \sim \langle x_1\rangle$, the amplitude of the motion, this term modifies the temperature excursion T_1 to include the fact that the gas instantaneously in the particular control volume at location x (in the Eulerian sense) came from a mean position of higher or lower mean temperature. Depending on the relative phasing of p_1 and u_1, this extra term may either raise or lower the amplitude of oscillating temperature at a given point along the duct.

Since the homogenous part of Eq. (18) is unchanged from Ref. 1, the current solution contains the same length scales

$$\delta_{\kappa D}^2 = \tfrac{1}{2}\delta_\kappa^2[1 + (1+\varepsilon)/L + \sqrt{[1+(1+\varepsilon)/L]^2 - 4/L}], \quad (24)$$

$$\delta_{D\kappa}^2 = \tfrac{1}{2}\delta_\kappa^2[1 + (1+\varepsilon)/L - \sqrt{[1+(1+\varepsilon)/L]^2 - 4/L}], \quad (25)$$

with $L \equiv (\delta_\kappa/\delta_D)^2 = k/\rho_m c_p D_{12}$, appearing in $h_{\kappa D}$ and $h_{D\kappa}$ due to the diffusion of heat and of mass for either the boundary-layer limit or a cylindrical duct; the functional forms of $h_{\kappa D}$ and $h_{D\kappa}$ are the same as those of h_ν, either exponential or Bessel depending on the geometry. In the boundary-layer limit, the δ's must be positive in order to satisfy the boundary condition that the solution remains finite as $y \to \infty$. For a cylindrical duct, the condition that the solution is finite at the center eliminates the Y_0 Bessel-function solutions. In that case, we can conveniently choose the δ's to be positive because J_0 is an even function of r.

Substitution of Eq. (23) in Eq. (18) and matching of h_ν terms gives

$$B = -\frac{\rho_m c_p}{p_1}\frac{\langle u_1\rangle}{\imath\omega}\frac{1}{1-f_\nu}\frac{\sigma}{(1-\sigma)(1-\sigma L) - \varepsilon\sigma} \times\left[(\sigma L - 1)\frac{dT_m}{dx} + \frac{\varepsilon T_m}{k_T'}\frac{dc_m}{dx}\right] \quad (26)$$

for arbitrary duct geometry, and with the Prandtl number $\sigma = (\delta_\nu/\delta_\kappa)^2 = \mu c_p/k$. For comparison with Eq. (33) of Ref. 2, this can be recast as

$$B = \frac{\imath e^{-\imath\theta}}{1-f_\nu}\frac{\sigma}{(1-\sigma)(1-\sigma L) - \varepsilon\sigma}[(\sigma L - 1)\Gamma_T + \varepsilon\Gamma_c], \quad (27)$$

where θ is the phase by which p_1 leads $\langle u_1\rangle$ and Γ_c is the same as in Ref. 2,

$$\Gamma_c = \frac{dc_m/dx}{(dc_m/dx)_{\text{sat}}} = \frac{dn_H/dx}{(dn_H/dx)_{\text{sat}}}, \quad (28)$$

where

$$\left(\frac{dc_m}{dx}\right)_{\text{sat}} = \frac{\gamma-1}{\gamma}k_T'\frac{|p_1|}{p_m}\frac{\omega}{|\langle u_1\rangle|}, \quad (29)$$

$$\left(\frac{dn_H}{dx}\right)_{\text{sat}} = \frac{\gamma-1}{\gamma}k_T\frac{|p_1|}{p_m}\frac{\omega}{|\langle u_1\rangle|}, \quad (30)$$

and Γ_T is given by Eqs. (2) and (3). For a parcel of gas executing standing-wave motion in a critical gradient of the correct sign with respect to the relative phasing of p_1 and u_1, the temperature of the gas would be approximately constant in time, ignoring the effect of viscosity on the velocity profile.

Finally, the coefficient C is obtained by substitution into the zero-flux boundary condition. For any duct geometry,

$$C = \left\{B\left[f_\nu\frac{(1-\sigma)}{\sigma} - f_{D\kappa}\left(\frac{\delta_\kappa^2}{\delta_{D\kappa}^2} - 1\right)\right] + f_{D\kappa}\left(\frac{\delta_\kappa^2}{\delta_{D\kappa}^2} - 1\right) + \frac{\imath e^{-\imath\theta}}{1-f_\nu}\Gamma_T\left[f_\nu + f_{D\kappa}\left(\frac{\delta_\kappa^2}{\delta_{D\kappa}^2} - 1\right)\right]\right\} \Big/ \left[f_{D\kappa}\left(\frac{\delta_\kappa^2}{\delta_{D\kappa}^2} - 1\right) - f_{\kappa D}\left(\frac{\delta_\kappa^2}{\delta_{\kappa D}^2} - 1\right)\right]. \quad (31)$$

This result can be made more compact for the boundary-layer limit as

$$C = C_{S\&S}\left\{1 - B\left[1 + \left(\frac{\sigma - 1}{\sqrt{\sigma}}\right)\frac{\delta_\kappa}{\sqrt{L}\delta_{\kappa D} - \delta_{D\kappa}}\right] + \frac{\iota e^{-\iota\theta}}{1 - f_\nu}\Gamma_T\left(1 + \sqrt{\sigma}\frac{\delta_\kappa}{\sqrt{L}\delta_{\kappa D} - \delta_{D\kappa}}\right)\right\}. \tag{32}$$

When $dT_m/dx=0$, this reverts directly to C as written in Eq. (35) of Ref. 2. When the concentration gradient is also set to zero, this expression clearly also reverts to the version of C found in the earlier article, Ref. 1.

Substituting T_1 into Eq. (15), we now obtain the oscillating concentration

$$c_1 = -\frac{p_1}{\rho_m c_p}\frac{k_T'}{\varepsilon T_m}\left\{\left(1 - \frac{1}{\sigma}\right)Bh_\nu + \left(1 - \frac{\delta_\kappa^2}{\delta_{\kappa D}^2}\right)Ch_{\kappa D} + \left(1 - \frac{\rho_m c_p}{p_1}\frac{\langle u_1\rangle}{\iota\omega(1-f_\nu)}\frac{dT_m}{dx} - B - C\right)\left(1 - \frac{\delta_\kappa^2}{\delta_{D\kappa}^2}\right)h_{D\kappa} + \frac{\rho_m c_p}{p_1}\frac{\langle u_1\rangle}{\iota\omega(1-f_\nu)}\frac{dT_m}{dx}h_\nu + \frac{\rho_m c_p}{p_1}\frac{\langle u_1\rangle}{\iota\omega(1-f_\nu)}\frac{\varepsilon T_m}{k_T'}\frac{dc_m}{dx}(1 - h_\nu)\right\}, \tag{33}$$

including the effect of a temperature gradient along the duct. This expression is correct for either the boundary-layer limit or the finite cylindrical tube, because Eq. (15) contains only even derivatives of T_1.

IV. THE SEPARATION FLUX TO SECOND ORDER

From Eq. (8) expressed in heavy mole fraction n_H instead of concentration c, the zeroth-order diffusive mole flux of the heavy component is

$$\dot{N}_{H,m} = -NAD_{12}\left(\frac{dn_H}{dx} + \frac{k_T}{T_m}\frac{dT_m}{dx}\right), \tag{34}$$

where A is the cross section of the duct and N is the molar density of the mixture. In the absence of bulk steady flow, the total mole flux of the heavy component through second order, including the effect of the axial temperature gradient, is then

$$\dot{N}_H = \dot{N}_{H,m} + \dot{N}_{H,2} = -NAD_{12}\left(\frac{dn_H}{dx} + \frac{k_T}{T_m}\frac{dT_m}{dx}\right) + \frac{\delta_\kappa}{4r_h}\frac{\gamma - 1}{\gamma}\frac{k_T}{R_{\text{univ}}T_m}|p_1||U_1|[F_{\text{trav}}\cos\theta + F_{\text{stand}}\sin\theta + F_{\nabla c}\Gamma_c + F_{\nabla T}\Gamma_T], \tag{35}$$

where R_{univ} is the universal gas constant, U_1 is the oscillating volumetric velocity, F_{trav} and F_{stand} were first introduced in Ref. 1, and $F_{\nabla c}$ is just F_{grad} from Ref. 2. Using the results of Sec. III, we can calculate the time-averaged second-order mole flux of the heavy component from

$$\dot{N}_{H,2} = \frac{m_{\text{avg}}}{m_H m_L}\frac{A\rho_m}{2}\Re\{\langle c_1\tilde{u}_1\rangle\}, \tag{36}$$

where tilde denotes the complex conjugate, m_H and m_L are the heavy and light molar masses, respectively, and $m_{\text{avg}} = n_H m_H + (1-n_H)m_L$ is the average molar mass. Because u_1 depends only on the momentum equation, all new dT_m/dx-dependent terms enter the mole flux linearly through c_1. Writing out all the terms explicitly,

$$\frac{A\rho_m}{2}\Re\{\langle c_1\tilde{u}_1\rangle\} = \frac{1}{2}\frac{k_T'/\varepsilon}{c_p T_m}\Re\left\{\frac{p_1\tilde{U}_1}{1-\tilde{f}_\nu}\left[-\left(\frac{\sigma-1}{\sigma}\right)B\langle h_\nu(1-\tilde{h}_\nu)\rangle - \left(1 - \frac{\delta_\kappa^2}{\delta_{\kappa D}^2}\right)C\langle h_{\kappa D}(1-\tilde{h}_\nu)\rangle - \left(1 - \frac{\delta_\kappa^2}{\delta_{D\kappa}^2}\right)\times\left(1 - \frac{\rho_m c_p}{p_1}\frac{\langle u_1\rangle}{\iota\omega(1-f_\nu)}\frac{dT_m}{dx} - B - C\right)\langle h_{D\kappa}(1-\tilde{h}_\nu)\rangle - \frac{\rho_m c_p}{p_1}\frac{\langle u_1\rangle}{\iota\omega(1-f_\nu)}\frac{dT_m}{dx}\langle h_\nu(1-\tilde{h}_\nu)\rangle - \frac{\rho_m c_p}{p_1}\frac{\langle u_1\rangle}{\iota\omega(1-f_\nu)}\frac{\varepsilon T_m}{k_T'}\frac{dc_m}{dx}\langle|1-h_\nu|^2\rangle\right]\right\}. \tag{37}$$

The last term in brackets, times $p_1\tilde{U}_1/(1-\tilde{f}_\nu)$, is purely imaginary so that it evaluates to zero in the $\Re\{\}$ and can be ignored. If $dT_m/dx \to 0$, then this expression reduces to Eq. (48) of Ref. 2. Since those contributions to the mole flux are already known, we can simplify the algebra by subtracting them from Eq. (37) in order to derive the contribution to the mole flux due to the temperature gradient alone. However, when $dT_m/dx \neq 0$, the definitions of B and C given here by Eqs. (27) and (31) contain dT_m/dx-dependent terms, so that one must take care in subtracting Eq. (48) of Ref. 2 from Eq. (37) above.

The flux can be evaluated making use of the identity

$$\langle h_i(1-\tilde{h}_j)\rangle = \frac{\delta_i^2}{\delta_i^2 + \delta_j^2}(f_i - \tilde{f}_j), \tag{38}$$

which holds true for any channel geometry.[9] If one considers only terms containing dT_m/dx, then one obtains from the portion in brackets above, after considerable work,

$$F_{\nabla T} = \frac{R}{\delta_\kappa}\frac{1}{|1-f_\nu|^2}\frac{\sigma}{(1-\sigma)(1-\sigma L) - \sigma\varepsilon}\times\Im\left\{\frac{f_\nu}{S}\left(\frac{\delta_{D\kappa}^2 - \delta_\kappa^2}{\delta_{D\kappa}^2 + \delta_\nu^2}f_{D\kappa} - \frac{\delta_{\kappa D}^2 - \delta_\kappa^2}{\delta_{\kappa D}^2 + \delta_\nu^2}f_{\kappa D} + \frac{(1+\sigma)LQ}{M}\tilde{f}_\nu + S\right) + \frac{1 - \sigma L - \sigma\varepsilon}{\sigma}G\right\}, \tag{39}$$

where R is the radius of the circular duct, and

$$S = \left(\frac{\delta_\kappa^2}{\delta_{D\kappa}^2} - 1\right)f_{D\kappa} - \left(\frac{\delta_\kappa^2}{\delta_{\kappa D}^2} - 1\right)f_{\kappa D}, \tag{40}$$

$$Q = \frac{\delta_{\kappa D}^2 - \delta_{D\kappa}^2}{\delta_\kappa^2}, \tag{41}$$

$$M = (1+\sigma)(1+\sigma L) + \varepsilon\sigma, \tag{42}$$

$$G = \frac{\sigma L Q}{SM} f_{\kappa D} f_{D\kappa} + \frac{\tilde{f}_\nu}{S}\left(\frac{f_{\kappa D}}{1+\delta_\nu^2/\delta_{D\kappa}^2} - \frac{f_{D\kappa}}{1+\delta_\nu^2/\delta_{\kappa D}^2}\right). \tag{43}$$

For parallel-plate geometry, use the hyperbolic-tangent expressions[6] instead of the Bessel expressions for f_i.

In the boundary-layer limit, $f_i = (1-\iota)\delta_i/2r_h$, so the result for $F_{\nabla T}$ reduces to just

$$-F_{\nabla T} = \frac{\sqrt{\sigma L}(1+\sqrt{L})(1+\sigma^2\sqrt{L}) + \sigma^{3/2}L + \sqrt{\sigma}\varepsilon - \frac{1}{\sqrt{\sigma}} + [\sqrt{L}(1-\sigma L-\sigma\varepsilon) - \sigma L(1+\sigma)]\frac{\delta_{\kappa D}+\delta_{D\kappa}}{\delta_\kappa}}{(1+\sqrt{L})[(1+\sigma)(1+\sigma L)+\sigma\varepsilon][(1-\sigma)(1-\sigma L)-\sigma\varepsilon]/\sigma}. \tag{44}$$

The various F parameters are plotted in Fig. 2(a) as a function of Ar mole fraction in a He–Ar mixture in the boundary-layer limit. Evidently $F_{\nabla T}$ is a fairly small contributor to the time-averaged mole flux for $|\Gamma_T| < 1$. Figure 2(b) shows the expected effect of this small contribution in our experiment's finite-diameter circular tube, for values of temperature gradient corresponding to $-0.8 < \Gamma_T < 0.8$, which is the range covered by our experiments.

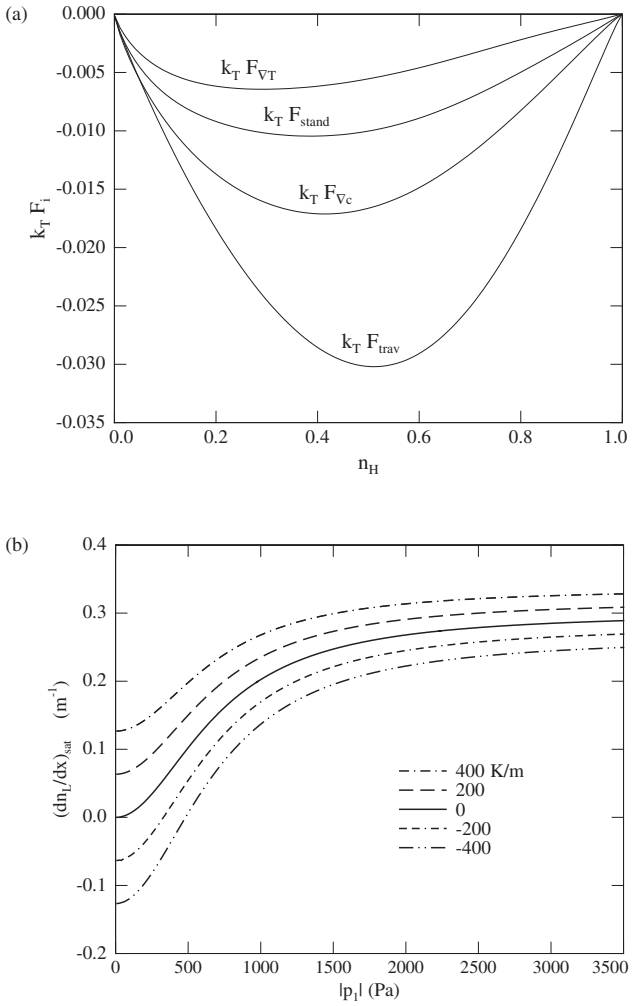

FIG. 2. (a) Comparison of $F_{\nabla T}$ to previously defined F's, for He–Ar in the boundary-layer limit. (b) The calculated mole-fraction gradient at which thermoacoustic mixture separation saturates (i.e., $\dot{N}_H = 0$) versus oscillating pressure amplitude for various values of the temperature gradient along a duct similar to those used in the experiments. These curves are calculated for 80 kPa 50–50 He–Ar mixtures in a 3.3 mm diameter tube at a frequency of 200 Hz. The calculation assumes traveling-wave phasing and a mean temperature of 300 K, and it uses the functional forms for a finite-diameter circular tube.

V. EXPERIMENTAL APPARATUS

The apparatus used to study the behavior of thermoacoustic mixture separation with an axial temperature gradient is a modified version of the apparatus used in the experiments on separation of neon isotopes[3] and on separation with continuous flow[4] of feedstock and products. Its geometry is shown in Fig. 3. In the current arrangement, the separation duct is a single 0.965 m length of stainless-steel tubing and fittings, with an inner diameter of 3.33 mm. The tubing was cut at three locations and joined back together by soldering into custom copper unions. These unions include side taps for attachment of microcapillaries carrying a small flux of the sample gas to a residual gas analyzer[10] (RGA) for concentration analysis. The unions also have side taps for connection to pressure transducers, which were used to verify the acoustic field in the duct. Small holes were drilled in the copper unions and thermocouple transducers were inserted to measure the local temperatures along the duct.

At the middle of the duct—its hottest point—it was necessary to thermally isolate the pressure transducer from the duct for two reasons. First, operating a transducer at elevated temperatures would have required calibration to evaluate its internal temperature compensation. Second, the temperature in the middle of the duct would often exceed the maximum operating temperature of the available transducer.[11] Therefore, this transducer was instead screwed into a small brass chamber with low dead volume, which was connected to the duct through 6 cm of stainless-steel capillary of 0.5 mm inner diameter. The brass chamber was water-cooled to maintain a temperature of about 300 K on the transducer. Calculations showed that this capillary and chamber did not significantly attenuate p_1 at the transducer.

The high operating temperatures in the middle of the duct also required that the microcapillaries to the RGA used to measure the He and Ar mole fractions be designed to withstand temperatures up to 575 K. The 5 cm lengths of glass microcapillary, with internal diameter 10 μm, were ep-

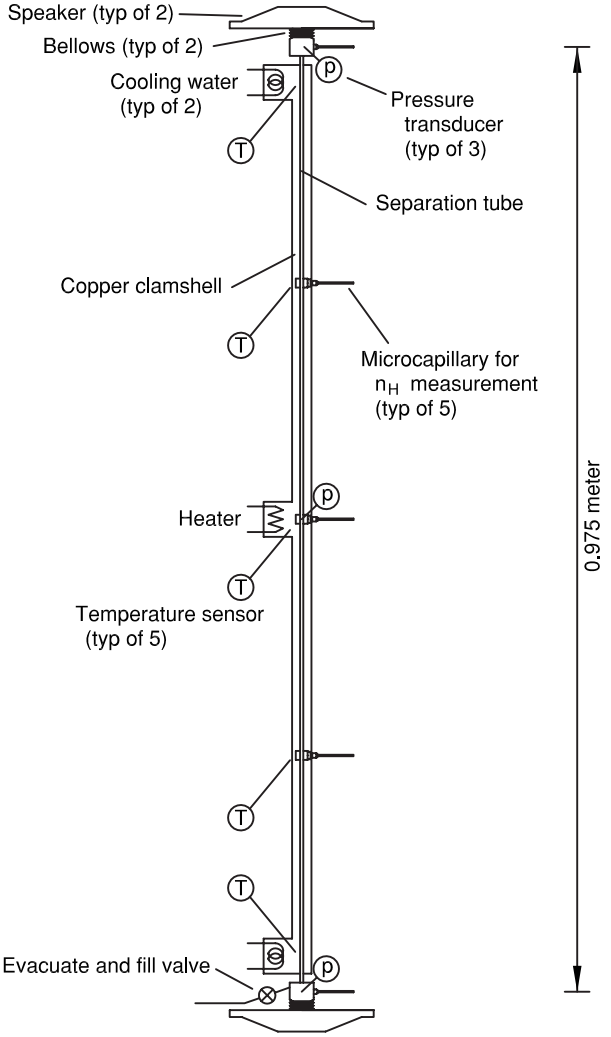

FIG. 3. The mixture-separation apparatus consists of a 3.3 mm diameter, 0.965 m long stainless steel tube, with hermetically sealed acoustic drivers at both ends. The connections to these drivers have ports for measuring the oscillating pressure and for withdrawing the mixture to a RGA, such that the length of the duct across which measurements are made is 0.975 m, slightly longer than the steel tube. The steel tube is sandwiched between two copper bars through which a circular groove was machined. This copper clamshell establishes the nearly linear thermal gradient along the duct, and it is held in place by the copper heatsinks at either end and by a copper clamp in the middle around which the heater is wound. The entire length of the copper clamshell is surrounded by fiberglass insulation (not shown) in order to minimize heat leaks to the surrounding room.

oxied into stainless-steel capillaries using a high-temperature epoxy.[12] These assemblies are attached to the copper unions using Swagelok connectors.

The duct, including the three copper unions, is enclosed in a clamshell formed from two 0.94 m long bars of 1 cm × 1 cm square copper. This clamshell serves as a thermal conductor to enforce a nearly linear temperature gradient along the duct. A ball-end mill was used to cut a groove lengthwise along one side of each bar to accommodate the circular duct. This clamshell was clamped onto the duct with water-cooled heat sinks at each end. The heat sinks cool the ends of the tube approximately to room temperature where they enter the acoustic drivers. Another copper clamp holds the clamshell together at the midpoint of the duct, and a heater tape is wound around this clamp. Heat is thus applied at the midpoint of the duct, so that the copper clamshell generates equal temperature gradients from the center to both ends of the tube, so we can study gradients both along and opposing the traveling wave at the same time in a single experiment.

Each end of the duct is connected to an acoustic driver composed of a hermetically sealed bellows attached to the dome of an electromagnetic speaker. The volume in each bellows is much larger than that of the separation tube itself. The duct is oriented vertically, and the gas mixture sample is introduced through a plug valve near the lower acoustic driver. Pressure transducers screwed directly into the duct near the drivers are used to set the drive voltages of the two speakers in order to achieve the desired pressure amplitudes and relative phases at the ends of the duct. The duct-end conditions on the oscillating pressure are chosen to give a traveling wave with a desired amplitude at the midpoint of the duct. These duct-end pressures are calculated numerically for a desired wave using DeltaEC.[13]

VI. RESULTS

Separation experiments were performed, starting from a spectroscopically verified 50–50 He–Ar mixture, for nine values of the temperature gradient—0, ±116, ±216, ±316, and ±416 K/m—corresponding to five mid-duct temperatures. For each value of the gradient, experiments were performed with traveling waves in the duct with nominal values for the oscillating pressure $|p_1|$ of about 1.0, 1.5, and 3.0 kPa at the midpoint of the duct. Before each experimental run, the temperature profile was established, the residual gas in the apparatus was pumped away to a pressure below 50 μm Hg, and the duct was filled with a fresh gas mixture to a pressure of 80 kPa, which is slightly above the typical atmospheric pressure in Los Alamos. When the duct's fill valve was left open too long, thermal diffusion between the duct and the fill manifold was observed to alter the mean concentrations in the duct over several minutes. This would result in the average concentration of the charge of gas in the duct not being 50–50 after the valve was closed. To minimize this effect, we first filled the filling manifold alone to a pressure calculated such that when the valve to the duct was momentarily opened, the duct would reach the desired equilibrium pressure given the applied thermal gradient. Then the final fill valve was opened just until the panel pressure stopped changing, which took less than 5 s.

After introducing the mixture, the acoustic wave was applied and the sample was allowed to separate for 1–3 h, depending on how long the concentrations were observed to change at the ends of the duct, which in turn depended on the amplitude of the wave and the temperature gradients along the duct. The mole fractions of He and Ar were then measured with the RGA for each of the five microcapillaries along the duct. The partial pressure of nitrogen was also recorded as a diagnostic for detecting leaks of air into the duct.

As noted in Ref. 4, the RGA is much more sensitive to argon than to helium, and the RGA-pumping system responds nonlinearly to the flow rate of the sample gas. In our experiments, the relative sensitivity of the RGA system to

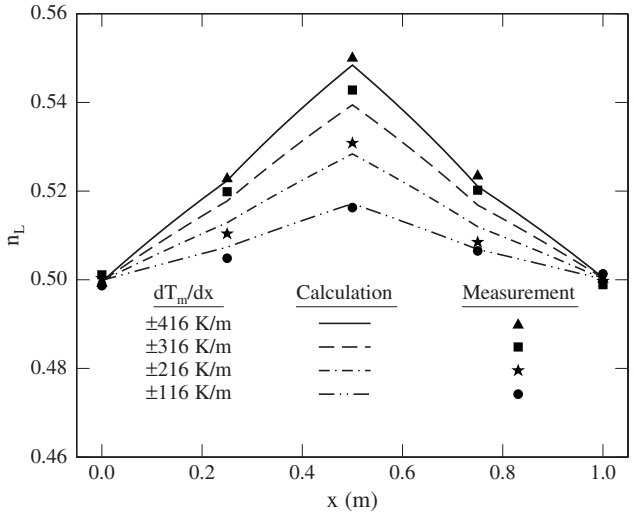

FIG. 4. Thermal diffusion for several applied gradients without acoustic excitation. Symbols are measurements and lines are calculations. At the ends of the duct, the temperature was held at 290 K by a recirculating chiller.

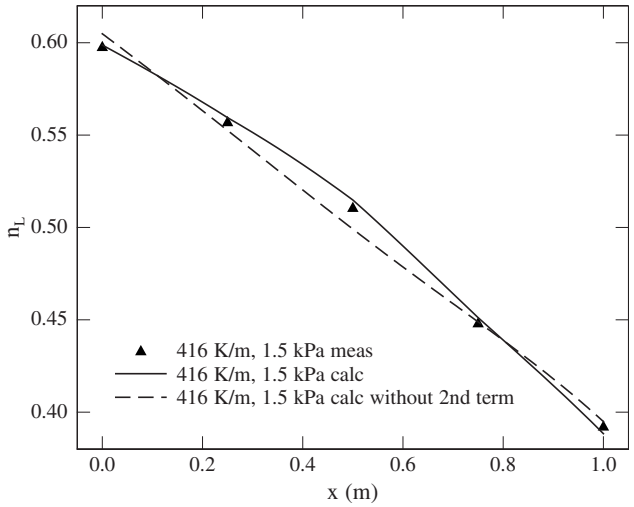

FIG. 5. Concentration versus position for a traveling wave propagating in the $-x$ direction with pressure amplitude $|p_1|=1.5$ kPa at the midpoint and a temperature gradient of ±416 K/m on either side of the midpoint. The solid triangles are measurements of helium mole fraction n_L at the five microcapillaries along the duct. The solid curve is a calculation (Ref. 13) using Eq. (45) and the dotted curve is a corresponding calculation using the theory of Ref. 2, which omits the dT_m/dx term in Eq. (45). The curves were calculated using as boundary conditions the values of acoustic pressure p_1 at each end of the duct and the requirement that the total helium concentration integrated over the apparatus was 0.5, because the fill valve was closed at the beginning of each experiment. Comparing the data and models in this way highlights the small differences in slope arising from the term with $F_{\nabla T}$.

helium versus argon is a function both of the flow rate of the gas through a microcapillary and of the true ratio of the concentrations of the gas mixture being sampled. For the present work, all five microcapillaries have very similar flow impedances so a single calibration might be expected to work for them all. However, the wide range of temperatures required by the experiment cause different flow rates through different microcapillaries, and therefore different relative sensitivities, in a single experiment. To account for this via calibration, the ratio of component partial pressures pp(Ar)/pp(He) reported by the RGA as gas flowed through a single, typical microcapillary was recorded with no sound wave and no temperature gradients, for different mixtures of He–Ar from 70–30 to 30–70 at 80 kPa and for mean pressures from 0 to 87 kPa in the 50–50 mixture. The relative sensitivity depended weakly, if at all, on argon concentration at fixed pressure, observed differences being less than the 0.01–0.02 accuracy of the measurement for the range of concentrations $(0.38 \leq n_L \leq 0.62)$ used in our separation experiments. However, the relative sensitivity varied by as much as 0.07 over the range of RGA partial pressures seen in our separation experiments. The relative sensitivity was nonlinear in the argon partial pressure, and at any given pressure it varied from day to day. To account for these problems, we used a fit to the calibration data to scale the relative sensitivity for each microcapillary based on the argon partial pressure measured there, and we forced a weighted average of the mole fractions (weighted by the volume distribution in the entire apparatus) to be exactly 0.5. This procedure reduced the uncertainty in the mole-fraction results to about 0.01, as confirmed in Fig. 4 for thermal diffusion without a sound wave. The thermal-diffusion ratio for He–Ar mixtures is well known,[14] so the calculated curves in Fig. 4 are a standard against which the data can be confidently compared.

When the ends of the tube are closed and the separation is allowed to run until it saturates, then $\dot{N}_H=0$ and the concentration gradient calculated from Eq. (35) is

$$\left(\frac{dn_H}{dx}\right)_{\text{sat}} = \left[\frac{\delta_\kappa}{4r_h}\frac{\gamma-1}{\gamma}\frac{k_T}{R_{\text{univ}}T_m}|p_1||U_1|(F_{\text{trav}}\cos\theta + F_{\text{stand}}\sin\theta) - \left(NAD_{12} - \frac{\delta_\kappa}{4r_h}NA\frac{|\langle u_1\rangle|^2}{\omega}F_{\nabla T}\right)\frac{k_T}{T_m}\frac{dT_m}{dx}\right] \Bigg/ \left[NAD_{12} - \frac{\delta_\kappa}{4r_h}NA\frac{|\langle u_1\rangle|^2}{\omega}F_{\nabla_c}\right]. \tag{45}$$

The change in the concentration gradient at saturation due to $dT_m/dx \neq 0$ therefore depends on the amplitude of the sound wave in the duct:

$$\Delta\left(\frac{dn_H}{dx}\right)_{\text{sat}} = -\frac{1-\frac{\delta_\kappa}{4r_h}\frac{|\langle u_1\rangle|^2}{\omega D_{12}}F_{\nabla T}}{1-\frac{\delta_\kappa}{4r_h}\frac{|\langle u_1\rangle|^2}{\omega D_{12}}F_{\nabla_c}}\left(\frac{k_T}{T_m}\frac{dT_m}{dx}\right). \tag{46}$$

The temperature gradient has the largest absolute effect when $|\langle u_1\rangle|=0$, because there is no thermoacoustic separation in that case but ordinary thermal diffusion still produces a concentration gradient. In that case, the dimensionless ratio in Eq. (46) is 1. As $|\langle u_1\rangle|\to\infty$, the acoustics dominates and the dimensionless ratio approaches $F_{\nabla T}/F_{\nabla c}$, which for a 50–50 He–Ar mixture is approximately 1/3, as shown in Fig. 2. For a 1.5-kPa traveling wave in our duct, the dimensionless ratio in Eq. (46) is about midway between these two extremes, so the thermoacoustic consequence of nonzero dT_m/dx is comparable with that of ordinary thermal diffusion. Figure 5 shows experimental data and calculations for this case.

For extensive comparison with the theory, separations were performed over a range of temperature gradients span-

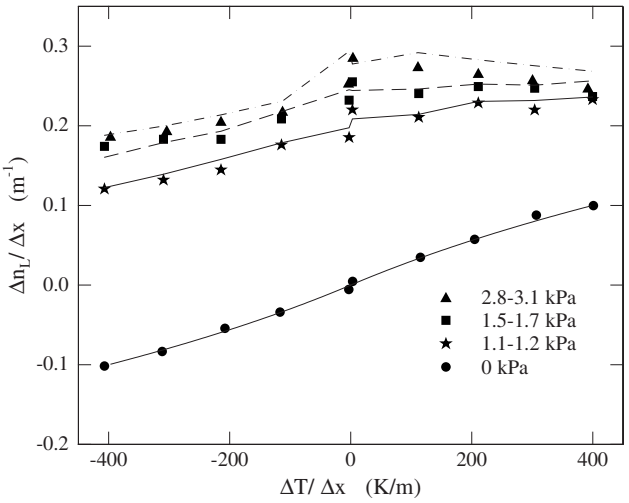

FIG. 6. A representation of all data and corresponding calculations, over the ranges $0 \leq |p_1| \leq 3.0$ kPa and $0 \leq |dT_m/dx| \leq 416$ K/m. The filled symbols are data for the finite-difference gradient in helium concentration versus the finite-difference gradient in temperature. The differences are from the ends of the duct to the middle, ignoring the measurements at the intermediate microcapillaries numbered 2 and 4. The curves are corresponding calculations, matched to the actual pressure amplitude of each measured point.

ning 0–416 K/m and over a range of oscillating pressure amplitudes $|p_1|$ from 0 to 3 kPa. The results are summarized in Fig. 6. This plot shows the gradients in concentration n_L versus gradients in temperature calculated between the middle of the duct, which was usually heated, and the end points of the duct, which were held at room temperature. In this way, each experiment at a different midpoint temperature or amplitude $|p_1|$ contributes two points to the graph. These points can be compared against the curves calculated using Eqs. (34)–(43) as implemented in DeltaEC,[13] for the experimentally measured temperatures and the pressure amplitudes recorded for each run. In general, the data roughly match the calculated curves.

An uncertainty of 0.01 in the measurements of n_L can result in an error of as much as $0.02/(0.5\ \text{m}) = 0.04\ \text{m}^{-1}$ in $\Delta n_L/\Delta x$. However, the highest-amplitude data show deviation from calculated values a little higher than this for $\Delta T/\Delta x > 0$, possibly due to turbulence. The Reynolds number of the oscillating flow is as high as 1600 at the high-amplitude end of the separation tube (the $\Delta T/\Delta x > 0$ end) based on $|U_1|$ and tube diameter. This is near the expected transition to turbulence for oscillating flow[15] in a tube with a diameter of the order of $10\delta_\nu$. The fact that the 3 kPa, $\Delta T/\Delta x > 0$ data here deviate from calculations more than do the 3 kPa, $\Delta T/\Delta x = 0$ data here and the 3 kPa, $\Delta T/\Delta x = 0$ data of Ref. 4 suggests that nonzero axial temperature gradients may affect the transition to turbulence.

Finally, evaluating Eq. (2) for the conditions of this experiment gives $(dT_m/dx)_{\text{crit}} \simeq 500$ K/m, only slightly above the experiment's highest gradients, 416 K/m. Thus, at temperature gradients near critical, we might have expected the acoustic separation to differ very little from the zero-acoustics separation for which axial thermal diffusion alone is responsible. The resolution of this paradox becomes apparent by setting $\dot{N}_H = 0$ and $dn_H/dx = (k_T/T_m)dT_m/dx$ in Eq. (35) and solving for dT_m/dx, obtaining

$$\frac{dT_m}{dx} = \frac{\gamma - 1}{\gamma} T_m \frac{|p_1|}{p_m} \frac{\omega}{|\langle u_1 \rangle|} \frac{F_{\text{trav}} \cos\theta + F_{\text{stand}} \sin\theta}{F_{\nabla c} - F_{\nabla T}}, \quad (47)$$

the actual temperature gradient for which the presence of the sound wave does not change dn_H/dx. Equation (47) differs from Eq. (2) by a factor depending on the four F's. For a standing wave in 50–50 He–Ar in the boundary-layer limit, Eq. (47) is nearly equal to Eq. (2), because $F_{\text{stand}} \simeq F_{\nabla c} - F_{\nabla T}$. But for a traveling wave in 50–50 He–Ar in the boundary-layer limit, Eq. (47) is 1500 K/m, about three times the value given by Eq. (2). This is the gradient at which all four sets of data in Fig. 6 would approach one another.

We retain Eq. (2) as the formal definition of $(dT_m/dx)_{\text{crit}}$ because it is simple, independent of tube size, and independent of the transport properties of the gas.

ACKNOWLEDGMENTS

This work was supported by Locally Directed R&D funds at Los Alamos National Laboratory. We are grateful to Mike Torrez and Carmen Espinoza for fabrication and assembly of the apparatus.

[1] G. W. Swift and P. S. Spoor, "Thermal diffusion and mixture separation in the acoustic boundary layer," J. Acoust. Soc. Am. **106**, 1794–1800 (1999); **107**(4), 2299 (2000); **109**(3) 1261 (2001).
[2] D. A. Geller and G. W. Swift, "Saturation of thermoacoustic mixture separation," J. Acoust. Soc. Am. **111**, 1675–1684 (2002).
[3] D. A. Geller and G. W. Swift, "Thermoacoustic enrichment of the isotopes of neon," J. Acoust. Soc. Am. **115**, 2059–2070 (2004).
[4] G. W. Swift and D. A. Geller, "Continuous thermoacoustic mixture separation," J. Acoust. Soc. Am. **120**, 2648–2657 (2006).
[5] R. C. Jones and W. H. Furry, "The separation of isotopes by thermal diffusion," Rev. Mod. Phys. **18**, 151–224 (1946).
[6] G. W. Swift, "Thermoacoustic engines," J. Acoust. Soc. Am. **84**, 1145–1180 (1988).
[7] L. D. Landau and E. M. Lifshitz *Fluid Mechanics* (Pergamon, New York, 1982).
[8] The hydraulic radius of a duct is defined as the ratio of its cross section to its perimeter. For a right circular cylinder, the hydraulic radius is equal to one-half of the cylinder radius.
[9] W. Pat Arnott, H. E. Bass, and R. Raspet, "General formulation of thermoacoustics for stacks having arbitrarily shaped pore cross sections," J. Acoust. Soc. Am. **90**, 3228–3237 (1991). See Eq. (45).
[10] RGA 100, Stanford Research Systems, Sunnyvale, CA, www.thinksrs.com (Last viewed February, 2009).
[11] Endevco Model 8510B-5, San Juan Capistrano, CA, www.endevco.com (Last viewed February, 2009).
[12] Aremco 526N, Valley Cottage, NY, www.aremco.com (Last viewed February, 2009).
[13] W. C. Ward, J. P. Clark, and G. W. Swift "Interactive analysis, design, and teaching for thermoacoustics using DeltaEC," J. Acoust. Soc. Am. **123**(5), 3546 (2008); software and user's guide available at www.lanl.gov/thermoacoustics/DeltaEC.html (Last viewed February, 2009). Version 6.2b3 included the segment type MIXTCIRC, which uses the equations derived in this paper.
[14] K. E. Grew and T. L. Ibbs, *Thermal Diffusion in Gases* (Cambridge University Press, Cambridge, 1952).
[15] G. W. Swift, *Thermoacoustics: A Unifying Perspective for Some Engines and Refrigerators* (Acoustical Society of America, Melville, NY, 2002), Fig. 7.4.